

# Thermal charge-density-wave transition and trion formation in the attractive SU(3) Hubbard model on a honeycomb lattice

Xiang Li,<sup>1</sup> Han Xu,<sup>1</sup> and Yu Wang<sup>1,\*</sup>

<sup>1</sup>*School of Physics and Technology, Wuhan University, Wuhan 430072, China*

We employ the determinant quantum Monte Carlo method to study the thermodynamic properties of the attractive SU(3) Hubbard model on a honeycomb lattice. The thermal charge density wave (CDW) transition, the trion formation, the entropy-temperature relation and the density compressibility are simulated at half filling. The CDW phase only breaks the lattice inversion symmetry on the honeycomb lattice and thus can survive at finite temperatures. The disordered phase is the thermal Dirac semi-metal state in the weak coupling regime, while in the strong coupling regime it is mainly a Mott-insulated state in which the CDW order is thermally melted. The formation of trions is greatly affected by thermal fluctuations. The calculated entropy-temperature relations exhibit prominent features of the Pomeranchuk effect which is related to the distribution of trions. Our simulations show that the density compressibility is still nonzero immediately after the CDW phase appears, but vanishes when the long-range order of trions forms.

## I. INTRODUCTION

With the high development of ultracold atom experiment, it is possible to study SU( $N$ ) ( $N > 2$ ) symmetries in alkali and alkaline-earth fermionic systems. In recent years, fermionic systems with SU( $N$ ) symmetries have attracted great attention from both theory [1–4] and experiment [5–12] communities in the context of ultracold atoms.

When the number of spin components  $N$  increases from 2 to  $N > 2$ , new physics may appear. SU(3) models should reveal the smallest difference between SU( $N$ ) systems and their SU(2) counterparts. The SU(3) symmetry can be realized by loading <sup>6</sup>Li atoms into the optical lattice [13–16]. In the optical lattices, the low-energy properties of the interacting fermionic atoms in three different hyperfine states can be described by the SU(3) Hubbard model [17], in which each hyperfine state is regarded as “flavor”.

The attractive SU(3) Hubbard model presents interesting properties. In Ref. [18], the dynamic mean-field theory (DMFT) study shows that on the Bethe lattice, the finite-temperature phase diagram of the attractive SU(3) Hubbard model includes the Fermi liquid phase, the color superfluid (CSF) phase and the trion phase. However, in the attractive SU(2) Hubbard model on the honeycomb lattice, the determinant quantum Monte Carlo (DQMC) study [19] presents that the superfluid state is degenerate to the charge density wave (CDW) state (dimer state) at half filling. Interestingly, when the number of flavors increases from 2 to 3, the projector quantum Monte Carlo (PQMC) study [20] shows that the CSF state is suppressed by the CDW state on the honeycomb lattice at half filling at zero temperature. Besides, the CDW state is the superposition of “on-site trion” state (one triply occupied sublattice plus one empty sublattice) and “off-site trion”

state (one doubly occupied sublattice plus one singly occupied sublattice).

In this paper, we study the thermodynamic properties of the half-filled attractive SU(3) Hubbard model on the honeycomb lattice through the DQMC simulations. We first study the semimetal-to-CDW phase transition through finite-size scalings. Then, we analyse how thermal fluctuations affect the formation of trions. We next calculate the entropy-temperature relation, which shows that the Pomeranchuk effect exists. The density compressibility is also calculated.

The rest of this paper is organized as follows. In Sec. II, the model Hamiltonian and the scheme of DQMC simulations are introduced. In Sec. III, the finite-temperature phase transition is studied; the trion formation is discussed; the Pomeranchuk effect is investigated; the density compressibility is researched. The conclusions and discussions are presented in Sec. IV.

## II. MODEL AND METHOD

### A. The SU(3) Hubbard model

The half-filled SU(3) Hubbard model takes the following form,

$$H = -t \sum_{\langle ij \rangle, \alpha} (c_{i\alpha}^\dagger c_{j\alpha} + \text{H.c.}) + U \sum_{i, \alpha < \beta} (n_{i\alpha} - \frac{1}{2})(n_{i\beta} - \frac{1}{2}), \quad (1)$$

in which  $t$  is the hopping amplitude;  $\langle ij \rangle$  denotes nearest-neighbor sites and the sum runs over sites of a honeycomb lattice;  $\alpha$  and  $\beta$  are the flavor indices running from 1 to 3;  $n_{i\alpha} = c_{i\alpha}^\dagger c_{i\alpha}$  is the particle number operator of flavor  $\alpha$  on site  $i$ ;  $U < 0$  describes the attractive on-site interaction. The chemical potential equals zero at half filling due to the particle-hole symmetry of the above Hamiltonian.

\* [yu.wang@whu.edu.cn](mailto:yu.wang@whu.edu.cn)

## B. The numerical method

We employ the non-perturbative DQMC method [21, 22]. The half-filled attractive SU(3) Hubbard model is sign-problem-free by using a special kind of Hubbard-Stratonovich (H-S) decomposition, which involves a special kind of auxiliary field [23–25] and maintains the SU(3) symmetry. Details about designing this special kind of H-S decomposition are explained in Ref. [20].

The important parameters of our DQMC simulations are summarized below. The time discretization parameter  $\Delta\tau$  is set between  $1/12$  and  $1/8$ , ensuring the convergence of the second-order Suzuki-Trotter decomposition and saving computing time. The  $2L \times L$  honeycomb lattice with  $L = 9$  is subjected to the periodic boundary condition, which preserves the translational symmetry. For a typical data point, we use 20 – 40 QMC bins each of which includes 400 – 500 warmup steps and 300 – 450 measurements. To study the finite-temperature phase transition through finite-size scalings, the  $2L \times L$  honeycomb lattices with  $L = 3, 6, 9, 12$  are simulated with 20 – 40 QMC bins, each bin including 300 – 500 warmup steps and 300 – 500 measurements.

## III. RESULTS

### A. The finite-temperature phase transition

We first define the order parameter of CDW phase:

$$D = \lim_{L \rightarrow \infty} \sqrt{\frac{1}{2L^2} S_{\text{CDW}}(L, \Gamma)}, \quad (2)$$

in which  $S_{\text{CDW}}(L, \Gamma)$  is the staggered charge structure factor defined at  $\Gamma$  point. The explicit form of  $S_{\text{CDW}}(L, \Gamma)$  is

$$S_{\text{CDW}}(L, \Gamma) = \frac{1}{2L^2} \sum_{i,j} (-1)^{i+j} C(i, j), \quad (3)$$

in which  $C(i, j) = \sum_{\alpha, \beta} \langle n_{i\alpha} n_{j\beta} \rangle$  is the density-density correlation function. In Ref. [19], the semimetal-to-CDW transitions are shown to occur in the half-filled attractive SU(2) Hubbard model on the honeycomb lattice. In the phase diagram, the CDW phase is degenerate to the superfluid phase. However, when the number of flavors increases from 2 to 3, the CDW phase suppresses the CSF phase because the CDW gap is larger than the CSF gap [20]. The CDW phase only breaks lattice inversion symmetry so the semimetal-to-CDW phase transitions should survive at finite temperatures. In this section, we will further investigate the finite-temperature CDW transitions of the attractive SU(3) Hubbard model.

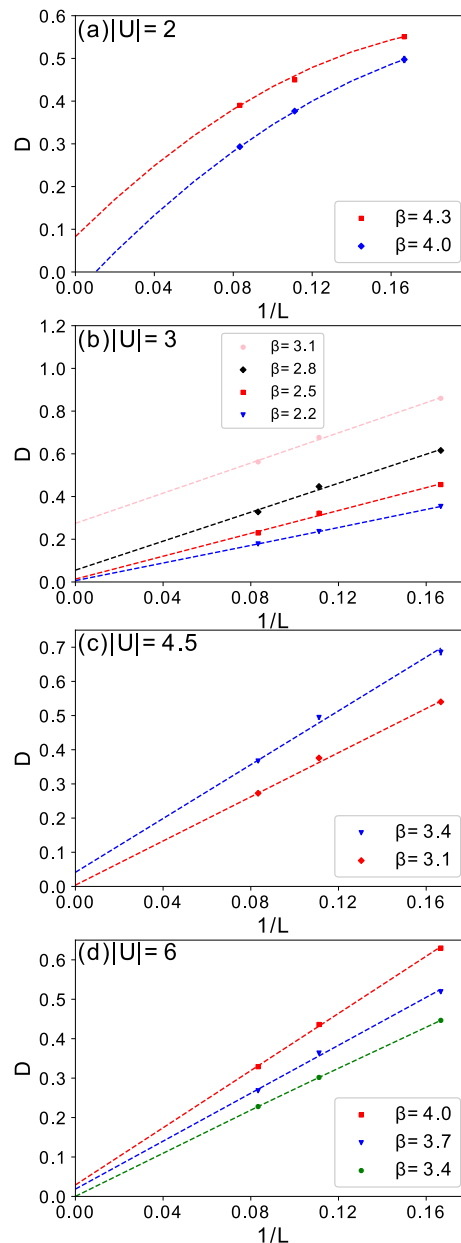


FIG. 1. Finite-size scalings of the CDW order parameter for the half-filled attractive SU(3) Hubbard model on the honeycomb lattice at different values of  $|U|$  and inverse temperature  $\beta$  close to the phase boundary. (a)  $|U| = 2.0$  with different values of  $\beta$ ; (b)  $|U| = 3.0$  with different values of  $\beta$ ; (c)  $|U| = 4.5$  with different values of  $\beta$ ; (d)  $|U| = 6.0$  with different values of  $\beta$ .

The finite-size scalings of the CDW order parameter are presented in Fig. 1. Based on these results, the finite-temperature phase diagram of the half-filled attractive SU(3) Hubbard model on the honeycomb lattice is plotted in Fig. 2. The transition temperature  $T_c$  increases with  $|U|$  in the interaction range  $1.52 \leq |U| \leq 3$  while it decreases as  $|U|$  further increases. The downward trend of  $T_c$  in the  $|U| \geq 3$  interaction range is explained by a perturbative analysis in Appendix. A. The

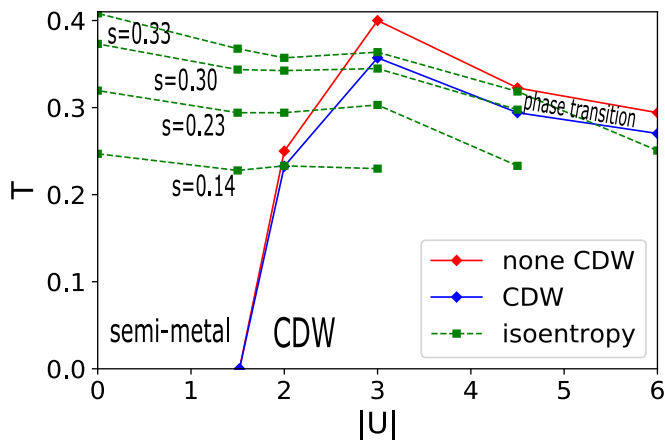


FIG. 2. The finite-temperature phase diagram of the half-filled SU(3) Hubbard model on a honeycomb lattice. The red and the blue lines represent the upper and lower boundaries of the transition temperatures determined by our DQMC simulations respectively. The zero-temperature result is extracted from Ref. [20]. With denser data points, the two boundaries should merge into one. The green dashed lines represent the isoentropy curves.

finite-temperature semimetal-to-CDW transitions are of second order, as is explained by a mean-field analysis in Appendix. B.

### B. Trion formation

The PQMC study [20] points out that the the ground state of our system is the superposition of on-site trion state and off-site trion state, as is shown in Fig. 3. The ground state is of long-range order: the order of on-site trions and off-site trions forms.

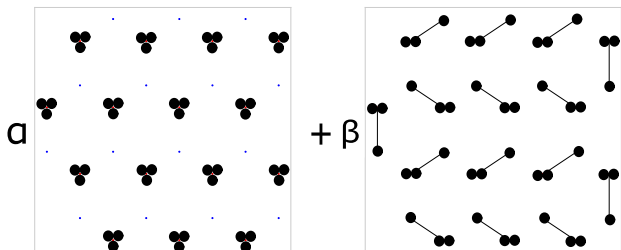


FIG. 3. The ground state: the superposition of on-site trion state and off-site trion state.  $\alpha$  and  $\beta$  are the superposition coefficient. Three black solid circles on a single site represent an on-site trion while a pair of black solid circles connected with one black solid circle by a black line segment represent an off-site trion. For simplicity, the picture is only drawn on the  $L = 3$  honeycomb lattice.

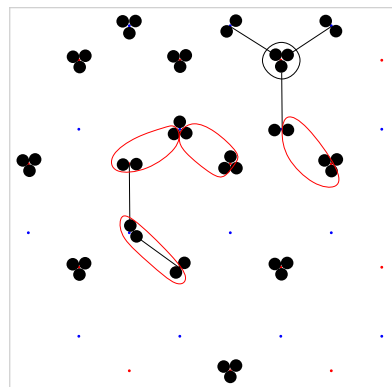


FIG. 4. One possible state of the system at relatively high temperatures. The distribution of off-site trions which contributes to  $P_3$  is labeled by a black ring; several distributions of trions contributing to  $P_{3\text{off}}$  are labeled by red rings.

However, the long-range order of the ground state should be destroyed by thermal fluctuations when the system is at relatively high temperatures at which thermal fluctuations are strong but not strong enough to break trions into free fermions. Hence, it is natural to assume that the possible states of the system at relatively high temperatures should be like Fig. 4. In these states, both on-site trions and off-site trions distribute randomly.

The possible states of the SU(3) system at relatively high temperatures can be understood by considering the correlation length of trions and the competition between on-site trions and off-site trions.

#### 1. Correlation length of trions

In this part, we study the correlation length of on-site and off-site trions by analysing the probability distribution [26, 27]

$$T(i, j) = \langle n_{i1}n_{i2}n_{j3} \rangle, \quad (4)$$

which measures the double occupancy of fermions with flavors  $\alpha = 1, 2$  on the reference site  $i$  provided that the fermion with the flavor  $\alpha = 3$  is on site  $j$ . We measure this observable in two cases: (1)  $j$  belongs to the same sublattice as  $i$ ; (2)  $j$  belongs to the different sublattice from  $i$ . The relations between  $T(i, j)$  and  $d(i, j)$  (the distance between  $i$  and  $j$ ) at various values of  $|U|$  and the inverse temperature  $\beta$  in these two cases are shown in Fig. 5 and Fig. 6 respectively.

$T(i, j)$  measures the correlation between a pair on site  $i$  and a particle on site  $j$  but it has more meanings in case (1) and case (2). At very low temperatures,  $T(i, j)$  does not change with  $d(i, j)$  obviously in both case (1) and case (2), which can be explained as follows. The ground state is the superposition of on-site trion state and off-site trion state and the superposition coefficient of on-site trion state is much larger than that of off-site trion

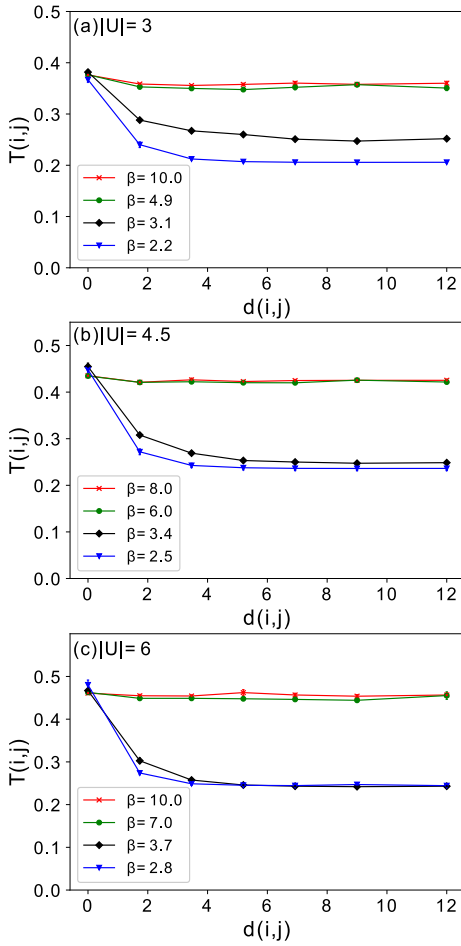


FIG. 5.  $T(i, j)$  versus  $d(i, j)$  (the distance between  $i$  and  $j$ ) at (a)  $|U| = 3$ , (b)  $|U| = 4.5$  and (c)  $|U| = 6$  at different inverse temperatures  $\beta$  in case (1). Very low temperatures  $T$  (very high inverse temperatures  $\beta$ ): (a)  $\beta=10.0$  and  $4.9$ ; (b)  $\beta=8.0$  and  $6.0$ ; (c)  $\beta=10.0$  and  $7.0$ . Relatively high temperatures  $T$  (relatively low inverse temperatures  $\beta$ ): (a)  $\beta=3.1$  and  $2.2$ ; (b)  $\beta=3.4$  and  $2.5$ ; (c)  $\beta=3.7$  and  $2.8$ .

state. In the ground state, every on-site trion locates on the same sublattice while for every off-site trion, a pair of particles locate on one sublattice and a particle locates on the other sublattice. The state of the system at very low temperatures should be very similar to the ground state. In case (1),  $T(i, j)$  is contributed by particles on the same sublattice so at very low temperatures,  $T(i, j)$  is only related to on-site trions. Because the long-range order of on-site trions exists at very low temperatures,  $T(i, j)$  should not change with  $d(i, j)$  obviously. Besides, due to the large superposition coefficient of on-site trion state, the value of  $T(i, j)$  is large in case (1). In case (2),  $T(i, j)$  is contributed by particles on different sublattices so at very low temperatures,  $T(i, j)$  is only related to off-site trions. Because long-range order of off-site trions exists at very low temperatures,  $T(i, j)$  should not change with  $d(i, j)$  obviously. However, due to the small superposition coefficient of off-site trion state, the value of  $T(i, j)$  is

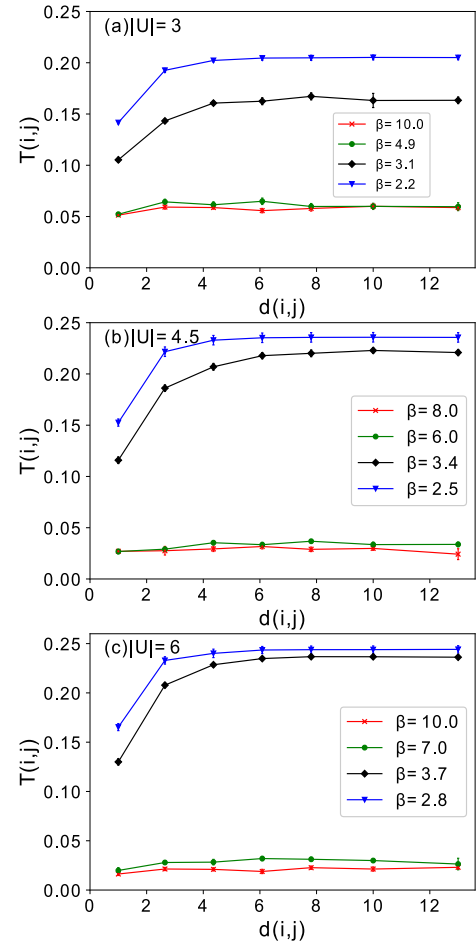


FIG. 6.  $T(i, j)$  versus  $d(i, j)$  (the distance between  $i$  and  $j$ ) at (a)  $|U| = 3$ , (b)  $|U| = 4.5$  and (c)  $|U| = 6$  at different inverse temperatures  $\beta$  in case (2). Very low temperatures  $T$  (very high inverse temperatures  $\beta$ ): (a)  $\beta=10.0$  and  $4.9$ ; (b)  $\beta=8.0$  and  $6.0$ ; (c)  $\beta=10.0$  and  $7.0$ . Relatively high temperatures  $T$  (relatively low inverse temperatures  $\beta$ ): (a)  $\beta=3.1$  and  $2.2$ ; (b)  $\beta=3.4$  and  $2.5$ ; (c)  $\beta=3.7$  and  $2.8$ .

small in case (2). The value of  $T(i, j)$  increases with  $|U|$  in case (1) while it decreases with  $|U|$  in case (2) at a given  $d(i, j)$ . This is because when  $|U|$  increases, the density of on-site trions rises while the density of off-site trions drops at very low temperatures.

At relatively high temperatures, in case (1),  $T(i, j)$  decreases with  $d(i, j)$ . This can be explained as follows. The long-range order of on-site trions at very low temperatures is gradually destroyed by thermal fluctuations and the correlation length of on-site trions becomes shorter than the lattice size. When  $d(i, j)$  increases,  $T(i, j)$  is less contributed by one on-site trion on site  $i$  and one on-site trion on site  $j$ . In case (2),  $T(i, j)$  increases with  $d(i, j)$ . This can be explained as follows. At relatively high temperatures, the long-range order of trions is destroyed by thermal fluctuations and the distributions of trions labeled by the black ring and the red rings in Fig. 4 appear.  $T(i, j)$  can not distinguish these distributions from off-site

trions so  $T(i, j)$  is much larger than the density of off-site trions at relatively high temperatures. Moreover, the correlation length of off-site trions becomes shorter than the lattice size. Hence, when  $d(i, j)$  increases,  $T(i, j)$  is less contributed by one off-site trion on site  $i$  and one off-site trion on site  $j$ .

Another important discovery is that the results in Fig. 6 support the existence of off-site trions rather than the existence of pairs plus free fermions [28].  $T(i, j)$  of a pair on site  $i$  with a free fermion on site  $j$  should not change with  $d(i, j)$  at relatively high temperatures since the free fermion can be on each site with equal probability but  $T(i, j)$  increases with  $d(i, j)$  at relatively high temperatures.

## 2. Competition between on-site trions and off-site trions

In this part, we analyse the competition between on-site trions and off-site trions from different perspectives. First, we analyse two observables based on  $T(i, j)$ :

$$P_3 = \frac{1}{N} \sum_i \langle n_{i1} n_{i2} n_{i3} \rangle \quad (5)$$

and

$$P_{3\text{off}} = \frac{1}{3N} \sum_{\langle ij \rangle} \langle n_{i1} n_{i2} n_{j3} \rangle, \quad (6)$$

in which  $N$  is the total number of sites;  $i$  runs over all sites;  $\langle ij \rangle$  denotes a pair of nearest-neighbor sites and  $i$  and  $j$  run over all sites too. The relations between these two observables and temperature  $T$  at different values of  $|U|$  are presented in Fig. 7 and Fig. 8 respectively.

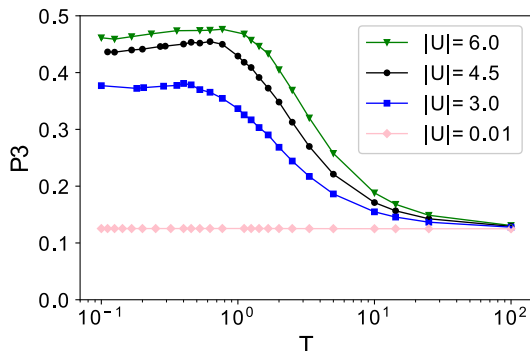


FIG. 7.  $P_3$  versus temperature  $T$  at different values of  $|U|$ . The lattice size is  $L = 9$ .

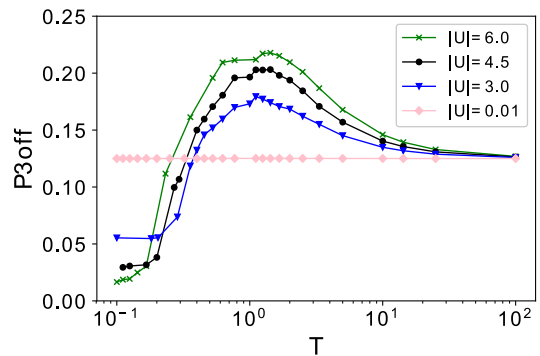


FIG. 8.  $P_{3\text{off}}$  versus temperature  $T$  at different values of  $|U|$ . The lattice size is  $L = 9$ .

At very low temperatures, thermal fluctuations are very weak and are not able to destroy the long-range order of on-site and off-site trions. Hence in this temperature regime,  $P_3$  mainly considers the density of on-site trions and should not change with temperature obviously and  $P_{3\text{off}}$  mainly considers the density of off-site trions and should not change with temperature obviously. At relatively high temperatures, the long-range order of trions is destroyed by strong thermal fluctuations. The distribution of trions labeled by the black ring in Fig. 4 contributes to  $P_3$  while the distributions of trions labeled by red rings contribute to  $P_{3\text{off}}$  greatly. Note that these distributions are neither on-site trions nor off-site trions. Hence,  $P_3$  is larger than the density of on-site trions and  $P_{3\text{off}}$  is much larger than the density of off-site trions at relatively high temperatures. As a result,  $P_3$  increases slightly with temperature and  $P_{3\text{off}}$  increases rapidly with temperature at relatively high temperatures. When the system is further heated up, both on-site trions and off-site trions split into free fermions. The saturated value of  $P_3$  and  $P_{3\text{off}}$  in the high temperature regime is  $0.5 \times 0.5 \times 0.5 = 0.125$ .

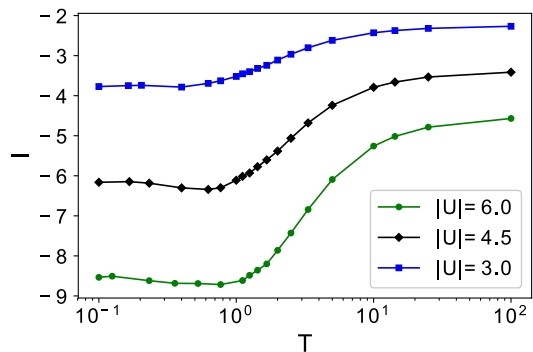


FIG. 9. The interaction energy per site  $I$  versus temperature  $T$  at different values of  $|U|$ . The lattice size is  $L = 9$ .

The competition between on-site trions and off-site trions is further supported by the relation between the interaction energy per site  $I$  and temperature  $T$ , as is shown in Fig. 9. When the system is cooled down from  $T = 100$



to around  $T = 1$ ,  $I$  decreases monotonically. This is because free fermions form on-site trions and off-site trions in this temperature regime. However, when the system is further cooled down,  $I$  increases slightly. This is because trions form long-range order gradually and the distributions of trions in Fig. 4 disappear (these distributions contribute to  $I$ ).

### C. The Pomeranchuk effect

In this section, We demonstrate the Pomeranchuk effect in the half-filled attractive SU(3) Hubbard model on a honeycomb lattice.

In ultracold atom experiment, it is entropy rather than temperature that is a directly measurable physical quantity [29]. We present below the entropy-temperature relations in the half-filled attractive SU(3) Hubbard model on a honeycomb lattice. The entropy per particle  $S(T)$  is calculated by:

$$\frac{S(T)}{k_B} = \frac{S(\infty)}{k_B} + \frac{E(T)}{T} - \int_T^\infty dT' \frac{E(T')}{T'^2}, \quad (7)$$

in which  $E(T)$  is the total energy per particle [30]. In the high temperature limit, there are  $2^3$  possible states on each site and thus  $S(T \rightarrow \infty) = k_B \frac{\ln 2^3}{3/2} = 2k_B \ln 2$  at half filling. However, the errorbars of  $E(T)$  affect the calculation of  $S(T)$  greatly when  $T < 1$  due to  $\frac{1}{T^2}$  in the integral, which is explained in Appendix. C. It is better to calculate  $S$  by the inverse temperature  $\beta$ :

$$\frac{S(\beta)}{k_B} = \frac{S(\beta = 0)}{k_B} + \beta E(\beta) - \int_0^{\frac{1}{T}} d(\beta) E(\beta). \quad (8)$$

Eq. 8 greatly reduces the affection of the errorbars of  $E(T)$  when  $T < 1$ . When  $|U| \leq 1.5$ , the system approaches the non-interacting limit and the errorbars of  $E(T)$  are nearly negligible. Hence, we can calculate  $S(T)$  accurately at very low temperatures. However, when  $|U| \geq 3$ , the errorbars of  $E(T)$  can not be neglected. At very low temperatures, large inverse temperature  $\beta$  amplifies the errorbars of  $E(\beta)$  in the second term in Eq. 8. Hence, we are only able to calculate  $S(\beta)$  accurately in the temperature regime  $T > 1/5.5$  when  $|U| \geq 3$ .

In Fig. 10, we present the entropy per particle  $S$  as a function of the temperature  $T$  at various values of  $|U|$ . The entropy curve with  $|U| = 0.01$  can be taken as the non-interacting entropy curve. The entropy curve with  $|U| = 3$  is so close to the entropy curve with  $|U| = 1.5$  below  $T = 1/2.8$ , which is reflected in the isentropy curves in the phase diagram Fig. 2: the isentropy curves are nearly horizontal when  $1.5 \leq |U| \leq 3$  below  $T = 1/2.8$ .

It is seen in Fig. 10 that, the SU(3) fermionic system can be driven to lower temperatures by increasing  $|U|$  adiabatically, which is called the Pomeranchuk effect.

We first consider the low specific entropy regime in which  $S(T, U)$  increases monotonically with  $|U|$  at a fixed

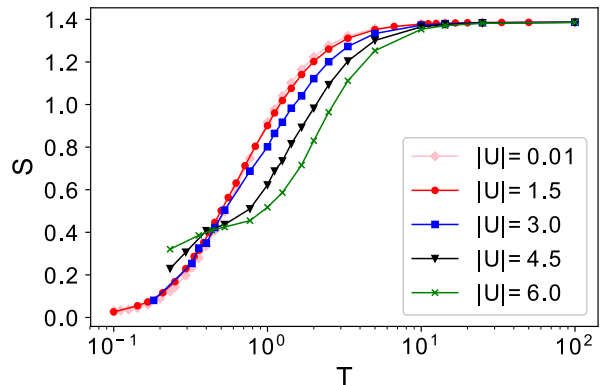


FIG. 10. Entropy per particle  $S$  as a function of temperature  $T$  at various values of  $|U|$  in the half-filled attractive SU(3) Hubbard model on the honeycomb lattice. The lattice size is  $L = 9$ .

temperature. When  $|U|$  is small, the system is in the semi-metal state. Its entropy is mainly contributed by fermions near the Dirac points, and thus is small due to the vanishing density of states. As  $|U|$  increases, the system enters into the CDW phase and its entropy mainly comes from possible distributions of off-site trions. The more disorderly off-site trions distribute, the higher the entropy is. Hence, the semi-metal phase is more ordered than the CDW phase at the same temperatures in the low specific entropy regime. In the CDW phase, the entropy increases with  $|U|$  at a given temperature. This can be explained by analysing the quantity

$$\Delta P_{3\text{off}}(T, U) = P_{3\text{off}}(T, U) - P_{3\text{off}}(T = 0, U), \quad (9)$$

which measures how disorderly off-site trions distribute at low temperatures and relatively high temperatures. In DQMC simulations, the data at zero temperature can not be gotten directly so we substitute  $P_{3\text{off}}(T = 0, U = -6)$  with  $P_{3\text{off}}(\beta = 10, U = -6)$  and  $P_{3\text{off}}(T = 0, U = -4.5)$  with  $P_{3\text{off}}(\beta = 9, U = -4.5)$  and  $P_{3\text{off}}(T = 0, U = -3)$  with  $P_{3\text{off}}(\beta = 10, U = -3)$ .  $\Delta P_{3\text{off}}(T, U)$  is mainly contributed by the distributions of trions labeled by colored rings in Fig. 4 in the low specific entropy regime. At zero temperature, both on-site trions and off-site trions form long-range order so there are no such distributions and  $\Delta P_{3\text{off}}(T = 0, U) = 0$ . At relatively high temperatures,  $\Delta P_{3\text{off}}(T, U)$  is larger when  $|U|$  is larger as can be gotten from Fig. 8. This means that off-site trions distribute more disorderly with larger  $|U|$  and the entropy of the system with larger  $|U|$  is larger. Due to the special dependence of  $S$  on  $|U|$ , increasing  $|U|$  adiabatically can drive the fermionic system to lower temperatures, as is shown in Fig. 10. In ultracold atom experiments, the interaction-induced cooling can be achieved in optical lattices via Feshbach resonances [29].

In the high specific entropy regime in which  $S(T, U)$  decreases monotonically with  $|U|$  at a fixed temperature, trions break up into free fermions gradually when the system is heated. The entropy mainly comes from possible

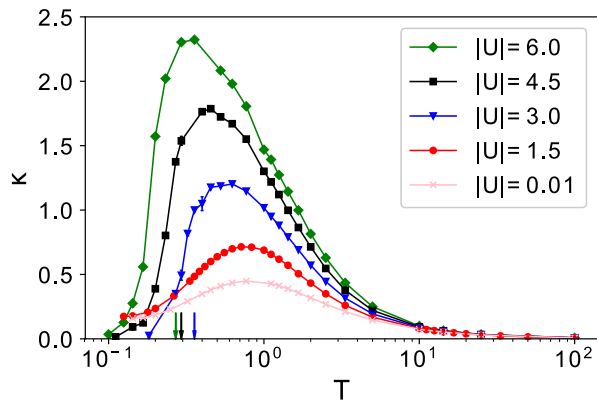


FIG. 11. The density compressibility  $\kappa$  versus temperature  $T$  at various values of  $|U|$  in the half-filled attractive SU(3) Hubbard model on the honeycomb lattice. The critical temperature  $T_c$  of the semimetal-to-CDW phase transition at different values of  $|U|$  are represented by arrows. The lattice size is  $L = 9$ .

distributions of free fermions. The attractive interaction makes trions harder to split up and thus reduces the number of free fermions. As a result, the number of possible distributions of free fermions decreases with  $|U|$  and  $S$  decreases with  $|U|$  at a fixed temperature in this entropy regime.

#### D. The density compressibility

The density compressibility is defined as

$$\kappa = \frac{\beta}{2L^2} \left( \left\langle \left( \sum_i n_i \right)^2 \right\rangle - \left\langle \sum_i n_i \right\rangle^2 \right), \quad (10)$$

which is connected with the global density fluctuations. It is an observable in cold atom experiments. At low temperatures, the vanishing of  $\kappa$  is a characteristic signature of the Mott insulating states [31, 32].

We present the relations between the density compressibility  $\kappa$  and the temperature  $T$  of the half-filled attractive SU(3) Hubbard model at different values of  $|U|$  on the honeycomb lattice in Fig. 11. At very high temperatures  $T \gg U$ ,  $\kappa(T)$  behaves like that of a classical ideal gas, i.e.,  $\kappa \approx \frac{1}{T}$ . Besides, increasing  $|U|$  while fixing  $T$  in this temperature regime enhances the compressibility due to the attractive interaction. When  $T < 1$ , if  $|U| \leq 1.5$ , the system remains in the semi-metal phase and  $\kappa$  decreases gradually towards zero from the maximum when the system is cooled down due to the vanishing density of states at very low temperatures; if  $|U| \geq 3$ ,  $\kappa$  decreases rapidly towards zero from the maximum after the system is cooled into the CDW phase. Note that the temperature  $T_{\text{mott}}$  at which  $\kappa = 0$  is lower than the critical temperature  $T_c$  of semimetal-to-CDW phase transition for  $|U| = 3, 4.5$  and 6. This is because when the system

just enters into the CDW phase, long-range order of trions has not developed yet. It is only when trions form long-range order, i.e, when  $\Delta P_{3\text{off}} = 0$  that the system becomes totally insulated and  $\kappa = 0$ .

## IV. CONCLUSIONS AND DISCUSSIONS

In summary, we have employed the DQMC simulations to study the SU(3) symmetry effects on thermodynamic properties of Dirac fermions which are described by the half-filled attractive SU(3) Hubbard model on a honeycomb lattice. We have studied the finite-temperature semimetal-to-CDW phase transition and then revealed the connection between trion formation and the Pomeranchuk effect and the density compressibility.

The CDW order only breaks a discrete symmetry and does exist in the thermal transition. The calculated entropy-temperature relations show that the  $S(T)$  curves with different  $|U|$  cross the non-interacting  $S(T)$  curve and  $S(T, |U| = 6) > S(T, |U| = 4.5) > S(T, |U| = 3)$  in the low specific entropy regime, which characterizes the presence of the Pomeranchuk effect. The entropy of the system with  $|U| \geq 3$  in the low specific entropy regime is mainly contributed by possible distributions of off-site trions. The density compressibility is still nonzero immediately after the CDW phase appears, but vanishes when the long-range order of trions forms.

## ACKNOWLEDGMENTS

This work is financially supported by the National Natural Science Foundation of China under Grants No. 11874292, No. 11729402, and No. 11574238. We acknowledge the support of the Supercomputing Center of Wuhan University.

### Appendix A: A perturbative explanation of the downward trend of $T_c$ in the $|U| \geq 3$ region

In the strong-coupling regime, we can take the interaction term in Eq. 1 as unperturbed Hamiltonian:

$$H_0 = -|U| \sum_{i,\alpha<\beta} (n_{i\alpha} - \frac{1}{2})(n_{i\beta} - \frac{1}{2}). \quad (A1)$$

$|\psi_m^0\rangle$ , the ground state of  $H_0$ , is highly degenerate: a half of the sites are occupied by on-site trions and these on-site trions distribute randomly in  $|\psi_m^0\rangle$ . The perturbation

$$H' = -t \sum_{\langle ij \rangle, \alpha} c_{i\alpha}^\dagger c_{j\alpha} + \text{H.c.} \quad (A2)$$

is the hopping term. The hopping term does not contribute in the first order. The effective Hamiltonian to

the second order is of the form:

$$H_{\text{eff}} = -|U| \sum_{i,\alpha < \beta} (n_{i\alpha} - \frac{1}{2})(n_{i\beta} - \frac{1}{2}) + \frac{t^2}{2|U|} \sum_{\langle ij \rangle, \alpha} n_{i\alpha} n_{j\alpha}. \quad (\text{A3})$$

The second term in Eq. A3 lifts the degeneracy of  $|\psi_m^0\rangle$ :  $|\psi_\alpha^0\rangle$ , the state in which on-site trions occupy one sublattice, is energetically favored.

With  $|U|$  increasing, the second term in Eq. A3 contributes less, which means that the energy difference between  $|\psi_\alpha^0\rangle$  and other excited states without CDW order becomes smaller. As a result, weaker thermal fluctuations can excite the system to a state without CDW order and  $T_c$  decreases with  $|U|$  in the strong-coupling regime. Furthermore, we can deduce that  $\lim_{|U| \rightarrow \infty} T_c = 0$ . The contribution of the second term in Eq. A3 is zero when  $|U| \rightarrow \infty$  and thus the energy difference between  $|\psi_\alpha^0\rangle$  and other excited states without CDW order disappears. As a result, infinitely small thermal fluctuations can excite the system to a state without CDW order.

### Appendix B: Mean-field analysis on the nature of the semimetal-to-CDW transition at finite temperatures

We first present a Ginzburg-Landau analysis on the nature of the semimetal-to-CDW phase transition at finite temperatures. As is pointed out in Ref. [20], the total GL free energy density  $f(\Delta)$  consists of analytic part

$$f_A(\Delta) = r_2 \Delta^2 + r_4 \Delta^4 \quad (\text{B1})$$

and nonanalytic part

$$f_N(\beta) \approx -\frac{6}{\beta} \int_0^\Lambda \frac{d^2 \vec{k}}{(2\pi)^2} [\ln(1 + e^{\beta E_k}) + \ln(1 + e^{-\beta E_k})]. \quad (\text{B2})$$

In Eq. B1 and Eq. B2,  $\Delta$  is the CDW order parameter defined as

$$\Delta = \frac{1}{2L^2 N} \sum_{i,\alpha} (-1)^i \langle c_{i\alpha}^\dagger c_{i\alpha} \rangle; \quad (\text{B3})$$

$\beta$  is the inverse temperature;  $\Lambda$  is the momentum cutoff;  $E_k = \sqrt{v^2 k^2 + (N-1)^2 U^2 \Delta^2}$  is the single-particle spectrum around each Dirac point at the mean-field level. In the definition of  $\Delta$  and  $E_k$ ,  $N$  is the number of flavors and  $k$  is the absolute value of the deviation from the location of the Dirac point.

Eq. B2 gives a nonanalytic term not included in  $f_A$  at zero temperature:

$$f_n = r_{3,n} |\Delta|^3. \quad (\text{B4})$$

Hence at zero temperature, the total free energy density is approximately  $r_2 \Delta^2 + r_{3,n} |\Delta|^3$ , which describes a second order transition with critical exponent 1.

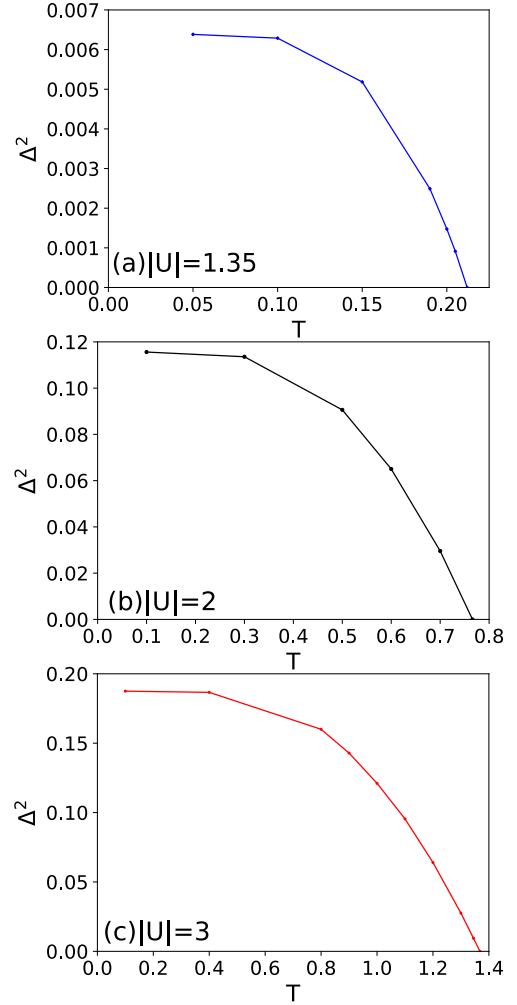


FIG. 12.  $\Delta^2$  versus temperature  $T$  for (a)  $|U| = 1.35$ ; (b)  $|U| = 2$ ; (c)  $|U| = 3$ . The lattice size is  $L = 99$ .

We then calculate the contribution of the nonanalytic part at finite temperatures using Eq. B2:

$$f_N(T) - f_N(T=0) = -\frac{6}{\pi\beta^3} \int_{\beta\Delta}^{+\infty} y \ln(1 + e^{-y}) dy. \quad (\text{B5})$$

If we take the limit of  $\Delta \rightarrow 0$  first and then set  $\beta$  at an arbitrarily low but still finite value, Eq. B5 contributes an extra nonanalytic term

$$\Delta f_n(T) = -r_{3,n} |\Delta|^3, \quad (\text{B6})$$

which precisely cancels  $f_n$ . As a result, the total GL free energy density  $f(\Delta)$  at finite temperatures only includes the analytic part  $f_A(\Delta)$ , which describes a second order transition with critical exponent  $\frac{1}{2}$ .

We then analyse the nature of the semimetal-to-CDW phase transition at finite temperatures by a mean-field calculation. According to Ref. [20], the mean-field Hamiltonian in the momentum space is

$$H_{\text{MF}} = \sum_{\vec{k}} \begin{pmatrix} a_{\vec{k}}^\dagger & b_{\vec{k}}^\dagger \\ \epsilon_{\vec{k}} & -2U\Delta \end{pmatrix} \begin{pmatrix} a_{\vec{k}} \\ b_{\vec{k}} \end{pmatrix}, \quad (\text{B7})$$



in which  $\epsilon_{\vec{k}} = -t \sum_{\vec{e}_j} e^{-i\vec{k} \cdot \vec{e}_j}$  and  $\vec{e}_j$  sums over  $\vec{e}_1 = (0, 1)$ ,  $\vec{e}_2 = (-\frac{\sqrt{3}}{2}, -\frac{1}{2})$  and  $\vec{e}_3 = (\frac{\sqrt{3}}{2}, -\frac{1}{2})$ ; the distance between nearest-neighbour sites is taken as the unit of length. Then the value of the CDW order parameter  $\Delta$  can be calculated self-consistently through definition Eq. B3.

The self-consistent results are shown in Fig.12. It is clear that the relation between  $\Delta^2$  and  $T_c - T$  is linear around  $T_c$  so  $\Delta$  is linear to  $(T_c - T)^{0.5}$  around  $T_c$ . The mean-field calculation agrees with our GL analysis.

### Appendix C: The affection of the errorbars of total energy at low temperatures

The errorbars caused by H-S decomposition in our simulations are proportional to  $o(\Delta_\tau^2)$  [20], which is much bigger than  $o(\Delta_\tau^4)$ , the approximate value of the errorbars caused by H-S decomposition in the SU(2N) Hubbard model. The affection of the errorbars of total energy can not be ignored when we calculate the specific entropy at low temperatures.

The calculation of the specific entropy involves the total energy per particle  $E$  as is defined in Eq. 7. The relations between the errorbars of total energy per site  $\Delta E$  divided by  $T^2$  and temperature  $T$  at temperatures lower than  $\frac{1}{1.3}$  at  $|U| = 6.0$  and  $|U| = 4.5$  are shown in Fig. 13.  $\frac{\Delta E}{T^2}$  is such a large number at low temperatures

that it makes the calculation of the entropy per particle  $S(T)$  unreliable in this temperature regime if we calculate  $S(T)$  by Eq. 7. Hence it is wiser to calculate  $S$  by the inverse temperature  $\beta$  rather than the temperature  $T$ .

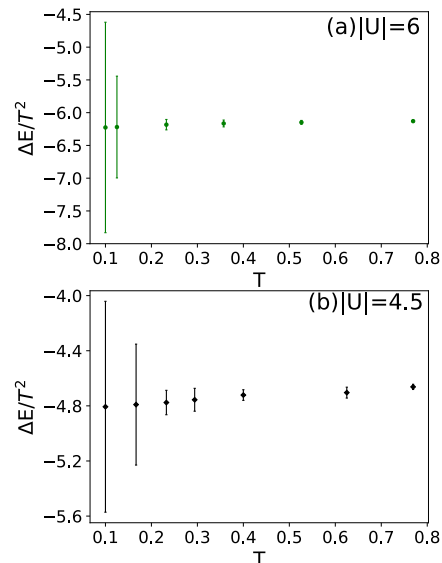


FIG. 13. The errorbars of total energy per site  $\Delta E$  divided by  $T^2$  versus temperature  $T$  at temperatures lower than  $\frac{1}{1.3}$  for (a)  $|U| = 6$  and (b)  $|U| = 4.5$  respectively.

- 
- [1] C. Wu, J.-p. Hu, and S.-c. Zhang, *Phys. Rev. Lett.* **91**, 186402 (2003).
- [2] C. Honerkamp and W. Hofstetter, *Phys. Rev. B* **70**, 094521 (2004).
- [3] C. Wu, *Phys. Rev. Lett.* **95**, 266404 (2005).
- [4] A. V. Gorshkov, M. Hermele, V. Gurarie, C. Xu, P. S. Julienne, J. Ye, P. Zoller, E. Demler, M. D. Lukin, and A. Rey, *Nature physics* **6**, 289 (2010).
- [5] S. Taie, Y. Takasu, S. Sugawa, R. Yamazaki, T. Tsujimoto, R. Murakami, and Y. Takahashi, *Physical Review Letters* **105**, 1 (2010).
- [6] B. J. Desalvo, M. Yan, P. G. Mickelson, Y. N. Martinez De Escobar, and T. C. Killian, *Physical Review Letters* **105**, 1 (2010).
- [7] S. Taie, R. Yamazaki, S. Sugawa, and Y. Takahashi, *Nature Physics* **8**, 825 (2012), arXiv:1208.4883.
- [8] F. Scazza, C. Hofrichter, M. Höfer, P. C. De Groot, I. Bloch, and S. Fölling, *Nature Physics* **10**, 779 (2014), arXiv:1403.4761.
- [9] X. Zhang, M. Bishof, S. L. Bromley, C. V. Kraus, M. S. Safronova, P. Zoller, A. M. Rey, and J. Ye, *science* **345**, 1467 (2014).
- [10] G. Pagano, M. Mancini, G. Cappellini, P. Lombardi, F. Schäfer, H. Hu, X. J. Liu, J. Catani, C. Sias, M. Inguscio, and L. Fallani, *Nature Physics* **10**, 198 (2014), arXiv:1408.0928.
- [11] M. A. Cazalilla and A. M. Rey, *Reports on Progress in Physics* **77** (2014), 10.1088/0034-4885/77/12, arXiv:1403.2792.
- [12] C. Hofrichter, L. Riegger, F. Scazza, M. Höfer, D. R. Fernandes, I. Bloch, and S. Fölling, *Physical Review X* **6**, 1 (2016), arXiv:1511.07287.
- [13] E. R. I. Abraham, W. I. McAlexander, J. M. Gerton, R. G. Hulet, R. Côté, and A. Dalgarno, *Physical Review A* **55**, R3299 (1997).
- [14] M. Bartenstein, A. Altmeyer, S. Riedl, R. Geursen, S. Jochim, C. Chin, J. H. Denschlag, R. Grimm, A. Simoni, E. Tiesinga, C. J. Williams, and P. S. Julienne, *Phys. Rev. Lett.* **94**, 103201 (2005).
- [15] T. Fukuhara, Y. Takasu, M. Kumakura, and Y. Takahashi, *Physical Review Letters* **98**, 1 (2007).
- [16] J. H. Huckans, J. R. Williams, E. L. Hazlett, R. W. Stites, and K. M. O'Hara, *Physical Review Letters* **102**, 1 (2009), arXiv:0810.3288.
- [17] C. Honerkamp and W. Hofstetter, *Physical Review Letters* **92**, 2 (2004).
- [18] K. Inaba and S. I. Suga, *Physical Review A - Atomic, Molecular, and Optical Physics* **80**, 2 (2009).
- [19] K. L. Lee, K. Bouadim, G. G. Batrouni, F. Hébert, R. T. Scalettar, C. Miniatura, and B. Grémaud, *Physical Review B - Condensed Matter and Materials Physics* **80**, 1 (2009).
- [20] H. Xu, Z. Zhou, X. Wang, L. Wang, and Y. Wang, *Physical Review Letters* **123**, 1 (2019), arXiv:1912.11233.
- [21] R. Blankenbecler, D. J. Scalapino, and R. L. Sugar,

- Physical Review D **24**, 2278 (1981).
- [22] J. E. Hirsch, *Phys. Rev. B* **31**, 4403 (1985).
- [23] L. Wang, Y. H. Liu, M. Iazzi, M. Troyer, and G. Harcos, *Physical Review Letters* **115**, 1 (2015).
- [24] Z. C. Wei, C. Wu, Y. Li, S. Zhang, and T. Xiang, *Physical Review Letters* **116**, 1 (2016), [arXiv:1601.01994](#).
- [25] Z. X. Li, Y. F. Jiang, and H. Yao, *Physical Review Letters* **117**, 1 (2016), [arXiv:1601.05780](#).
- [26] A. Kantian, M. Dalmonte, S. Diehl, W. Hofstetter, P. Zoller, and A. J. Daley, *Physical Review Letters* **103**, 1 (2009), [arXiv:0908.3235](#).
- [27] J. Pohlmann, A. Privitera, I. Titvinidze, and W. Hofstetter, *Physical Review A - Atomic, Molecular, and Optical Physics* **87**, 1 (2013).
- [28] J. Pohlmann, A. Privitera, I. Titvinidze, and W. Hofstetter, *Physical Review A - Atomic, Molecular, and Optical Physics* **87**, 1 (2013).
- [29] I. Bloch, J. Dalibard, and W. Zwerger, *Reviews of Modern Physics* **80**, 885 (2008).
- [30] Z. Zhou, D. Wang, C. Wu, and Y. Wang, *Physical Review B* **95**, 1 (2017).
- [31] U. Schneider, L. Hackermüller, S. Will, T. Best, I. Bloch, T. A. Costi, R. W. Helmes, D. Rasch, and A. Rosch, *Science* (2008), [10.1126/science.1165449](#), [arXiv:0809.1464](#).
- [32] P. M. Duarte, R. A. Hart, T. L. Yang, X. Liu, T. Paiva, E. Khatami, R. T. Scalettar, N. Trivedi, and R. G. Hulet, *Physical Review Letters* **114**, 1 (2015), [arXiv:1409.8348](#).